Photophysical Processes Involved within the Anisole−Thioindoxyl Dyad System

Sudeshna Bhattacharya,[†] Tarun K. Pradhan,[‡] Asish De,[‡] Shyamal Roy Chaudhury,[§] Avijit K. De,[||] and Tapan Ganguly*[,†]

Department of Spectroscopy, Indian Association for the Cultivation of Science, Jadavpur, Kolkata 700032, West Bengal, India, Department of Organic Chemistry, Indian Association for the Cultivation of Science, Jadavpur, Kolkata 700032, West Bengal, India, Department of Chemistry, Dinabandhu Andrews College, Garia, Kolkata, West Bengal, India, and Department of Engineering Science, Haldia Institute of Technology, Haldia-721657, Midnapore East, India.

Received: November 13, 2005; In Final Form: March 2, 2006

The photophysical properties and the nature of the photoinduced electron transfer (PET) reactions within a synthesized anisole (A)−thioindoxyl (T) dyad system (24MBTO) have been studied by electrochemical, steady-state, and time-resolved spectroscopic techniques. Computations on the dyad were performed both in gas phase as well as solvent environment by TD-DFT method with B3LYP density function. The geometry optimization calculation of 24MBTO was done by 6−311G(d,p) basis function set implemented in the Gaussian package. The theoretical values of singlet vertical excitation energies were found to correlate well with the experimentally observed ones. The electrochemical measurements indicate the possibility of occurrence of PET reactions within 24MBTO between the linked redox centers A and T. Both steady-state and time-resolved spectroscopic measurements on the novel synthesized 24MBTO dyad demonstrate the formations of the two types of isomeric species: Z- and E- forms, resulted from the charge separation reactions. From the detailed studies it reveals that the present thioaurone may behave as a versatile photoswitchable system. It has been hinted that the loss process (charge recombination) within 24MBTO could possibly be prevented by incorporating it within the hydrophobic cavity of β-cyclodextrin (βCD).

1. Introduction

Photoinduced electron transfer (PET)[1] is one of the most important processes in photosynthesis, photoimaging, optoelectronic, and other microelectronic devices. Investigations on PET processes[2−27] within the well-defined artificial photosynthetic systems may lead to further insights into the mechanisms of natural photosynthesis. Lately, comparative studies[26] were made between intermolecular and intramolecular ET reactions within 4-methoxy benzo[*b*]thiophene (4MBT) donor and *p*-chloroacetophenone (PCA) acceptor by using steady-state and laser-flash photolysis techniques, and these studies were extended in β-cyclodextrin (βCD)[27] microenvironment. The primary aim of this research is to build efficient artificial photosynthetic devices (model donor−acceptor-linked bichromophoric and multichromophoric systems) where charge separation reactions will occur relatively much faster than the charge recombination process. It has been shown that the survival duration of charge separated species before recombination depends somewhat on the nature of the linkage, saturated or unsaturated. This duration could be significantly enhanced by incorporating the whole bichromophore within the nonpolar cavity of βCD[27]. Thus, this cyclodextrin microenvironment could serve as a suitable medium in which one of the key requirements for the artificial photosynthesis has been achieved.

In the present investigation, electrochemical, steady-state, and time-resolved spectroscopic measurements were made on the novel synthesized dyad 2-(4-methoxy-benzylidene)-benzo[*b*]-thiophen-3-one (24MBTO) where anisole (A) and thioindoxyl (T) are connected by an unsaturated linker (Figure 1). From the present detailed studies on 24MBTO, observations of two different isomers (E- and Z-types, Figure 1a) were made both in the ground and excited electronic states resulted from the charge separation reactions within the donor A and the acceptor T. Both the steady-state and time-resolved spectroscopic investigations were carried out in the highly polar ($\epsilon_s \approx 37.5$) solvent acetonitrile (ACN) and βCD microenvironment to reveal the nature and structures of these isomers formed within the linked system. By using time-dependent density functional theory (TD-DFT) with B3LYP/6-311G(d,p) method, we computed optimized geometry in the ground state of 24MBTO along with vertical excitation energies both in the gas phase and ACN environment by IEEPCM model. The computed data have been compared with the experimentally observed values. The results obtained from the present studies are described in this paper.

2. Experimental Section

2.1. Materials. *Synthesis and Characterization.* The target molecule, 2-(4-methoxy-benzylidene)-benzo[*b*]thiophen-3-one (24MBTO), which is a member of a class of compounds known as thioaurones, was synthesized from thiosalisylic acid, which was first converted into its diethyl amide by sequential conversion into its acid chloride followed by treatment with *N*,*N*-diethylamine in benzene to afford thiosalicylamide. The latter

* To whom correspondence should be addressed. Phone: +91-33-2473-4971 ext 253; Fax: +91-33-2473-2805; E-mail: sptg@mahendra.iacs.res.in, tapcla@rediffmail.com.

[†] Department of Spectroscopy, Indian Association for the Cultivation of Science.

[‡] Department of Organic Chemistry, Indian Association for the Cultivation of Science.

[§] Dinabandhu Andrews College.

[||] Haldia Institute of Technology.

10.1021/jp056556w CCC: $33.50
Published on Web 04/01/2006

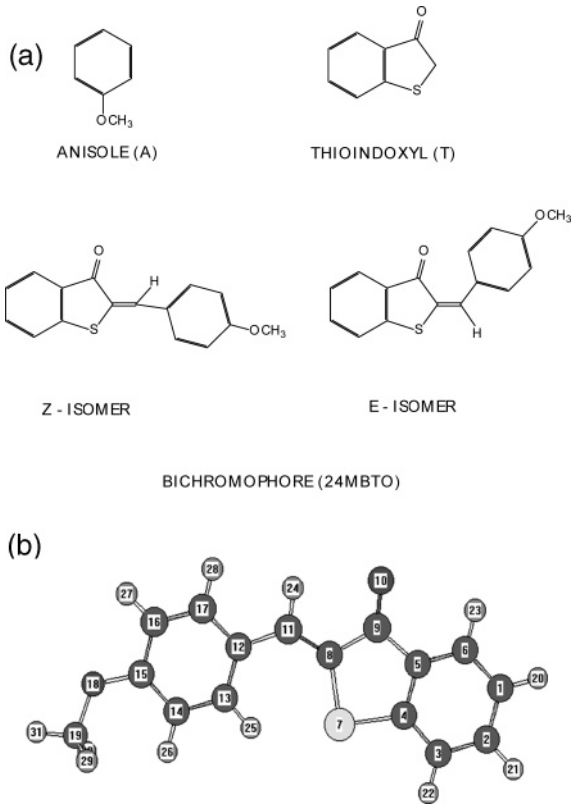

Figure 1. (a) Structures of 24MBTO. (b) 6−311G(d,p) optimized geometry of 24MBTO. 10,18: Oxygen; 7: sulfur; 1−6,8,9,11−17,19: carbon; 20−31: hydrogen.

was converted into *o*-methylsulfanyl *N*,*N*-diethyl amide by refluxing with NaH in THF and then stirring with methyliodide. When this *o*-methylsulfanyl tertiary amide was treated with anisaldehyde (1.2 equiv) in the presence of 2.5 equiv of LDA at 0 °C, usual acidic work up afforded 2-(4-methoxy-benzylidene)-benzo[*b*]thiophen-3-one as a dark-yellow solid having mp 145 °C; IR (KBr) υ_{max}: 1670.2, 1560.3, 1596.9, 1512.1, 1448.4, 1286.4, 1296.1, 1311.5, 1182.3, 1056.9, 1070.4, 1020.3, 1263.3, 821.6, 734.8, 677.0, 532.3 cm^{-1}; ^1H NMR ($CDCl_3$, 300 MHz,) δ_{ppm}: 7.95−7.92 (2H, m), 7.69−7.65 (2H, m), 7.59−7.49 (2H, m), 7.31−7.26 (1H, m), 7.02−6.99 (2H, m), 3.87 (3H, s, OCH_3); ^{13}C NMR ($CDCl_3$, 75 MHz,) δ_{ppm}: 188.4, 161.1, 145.8, 135.7, 134.8, 133.6, 132.9, 132.9, 130.6, 127.6, 126.9, 125.3, 123.7, 114.4, 114.4, 55.3.

2.2. Other Chemicals Used. The solvent ACN (SRL) of spectroscopic grade was distilled under a vacuum following the standard procedure and tested before use to detect any impurity emission in the concerned wavelength region. βCD (Aldrich) and methanol (MeOH) (E Merck, Germany) of spectroscopic grade were used as received. Water was deionized using a Millipore Milli-Q system. The solutions were prepared by dissolving the appropriate amount of βCD in water. Because of the low solubility in water, 24MBTO was dissolved in pure MeOH and added to the water solution of βCD; this is a well-known procedure implemented in earlier cases.[27,28] The final methanol concentration in a mixture was <2%(v/v).

2.3. Spectroscopic Apparatus. At the ambient temperature (296 K), steady-state UV−vis and fluorescence emission spectra of dilute solutions (10^{-4}−10^{-6} mol dm^{-3}) of the samples were recorded using 1-cm path length rectangular quartz cells by means of an absorption spectrophotometer (Shimadzu UV−Vis 2101PC) and F-4500 fluorescence spectrophotometer (Hitachi), respectively. For lifetime measurements, the sample was excited at 405 nm using a picosecond diode laser (IBH Nanoled-07) in an IBH Fluorocube apparatus. The emission was collected at a magic angle polarization using a Hamamatsu MCP photomultiplier (5000U-09). The time correlated single photon counting (TCSPC) setup consists of an Ortec 9327 CFD and a Tennelec TC 863 TAC. The data are collected with a PCA3 card (Oxford) as a multichannel analyzer. The typical fwhm of the system response using a liquid scatterer is about 80 ps. The fluorescence decays were deconvoluted using IBH DAS6 software.

2.4. Computational Methods. The geometry optimization calculation of 24MBTO was done by 6−311G(d,p)[29−31] basis function set implemented in the Gaussian package.[32] Molecular coordinates were obtained from minimum energy geometry using Chemoffice molecular modeling software. For vertical excitation energy of electronic spectra, the TD-DFT method was used with the B3LYP function. Calculations are carried out for the vacuum/gas phase and ACN environment. The solvation effect was simulated by the TD-DFT excitation energy and using continuum model IEFPCM (polarization continuum model) for excited-state energy. For singly excited electronic spectra, configuration interactions (CI) were carried out by 10 × 10 occupied and unoccupied molecular orbital.

2.5. Electrochemical Measurements. The redox potentials of the reactants A and T were measured in ACN solvent by cyclic voltammetric method using the PAR model VersaStat II electrochemistry system. Three electrode systems including Ag/AgCl as standard were used in the measurements. Tetraethylammonium perchlorate (TEAP) was used as the supporting electrolyte.

3. Results and Discussion

3.1. *(i) Electrochemical Measurements.* From the measurements of the oxidation potential of A (+1.24 V) and reduction potential of T (−1.04 V), it appears that there is a possibility of occurrence of photoinduced electron-transfer reactions between the electron-donor A and the acceptor T when either of the reactants are excited. The thermodynamic parameter $\Delta G°$, determined from the well-known Rehm−Weller relation,[1c] was found to be −1.12 eV (exergonic) in ACN medium. Thus, 24MBTO, where A and T have been connected by a linker, may serve as a good dyad system. The detailed photophysical investigations, by steady-state and time-resolved spectroscopic techniques, on this system are described below.

(ii) Measurement of UV−Vis Spectra. In ACN solution and at the ambient temperature, the UV−vis spectra of the mixture of the donor A and the acceptor T appear to be just a superimposition of the corresponding spectra of each reactant (Figure 2). This indicates the lack of formation of any intermolecular charge-transfer (CT) complex within the above reacting species in the ground state. The similar observations were made when the concentrations of both the donor A and the acceptor T were varied from $\times 10^{-5}$ to $\times 10^{-3}$ mol dm^{-3}. But the nature of the UV−vis absorption spectra changes significantly when these two reacting species are connected by an unsaturated olefinic linker, i.e., in the case of the present bichromophore, 2-(4-methoxy-benzylidene)-benzo[*b*]thiophen-3-one (24MBTO), where A is attached with benzo[*b*]thiophen-3-one ring by an unsaturated bond. An observed broad long wavelength absorption band spanning between 375 and 500 nm (Figure 3) appears to be responsible for the formation of the ground-state intramolecular CT complex of A and T, the two redox partners present within 24MBTO. This observation demonstrates that the mutual orientation between the linked donor and acceptor moieties may facilitate the formation of such ground-state complex. Further, NMR studies confirm that the

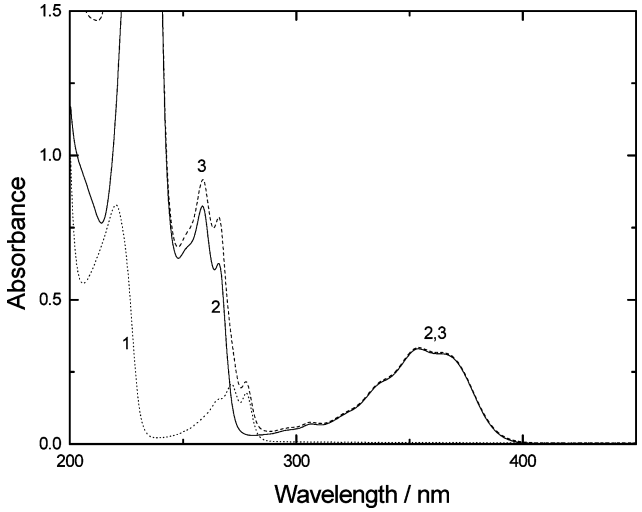

Figure 2. Steady-state electronic absorption spectra in ACN of (1) A; (2) T; (3) mixture of A and T at the ambient temperature.

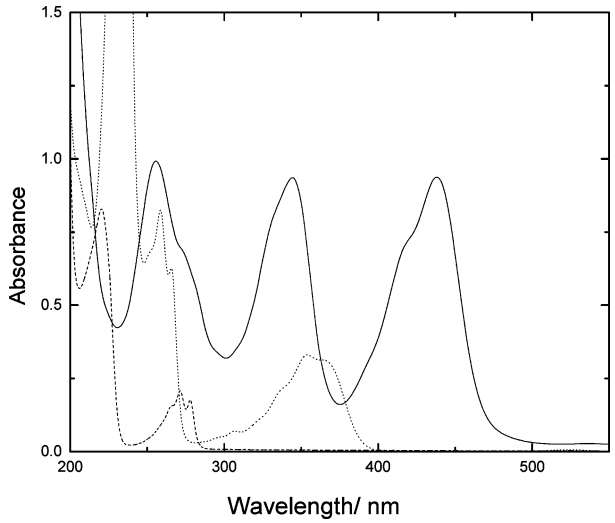

Figure 3. Steady-state electronic absorption spectra in ACN of A (dashed line), T (dotted line), and 24MBTO (solid line) at the ambient temperature.

structure of this complex is similar to that of Z-type isomer of 24MBTO (Figure 1a).

(iii) Ground-State Calculations: Molecular Geometry and Ground-State Dipole Moment (a) Molecular Geometry. The geometry optimization calculation of 24MBTO was done by B3LYP/6-31G(d,p) basis function set implemented in the Gaussian package. The simulation optimizes bond length, bond angles, and dihedral angles. Some selected bond length and bond angles of the spacer part of the bichromophore molecule 24MBTO are shown in Table 1. From the ground-state calculation it was revealed that the bichromophore has C_1 symmetry with planar structure (Figure 1b). From the optimized geometry computation of 24MBTO, it shows that the molecular structure of this bichromophore closely resembles that of its Z-isomeric form (Figure 1b). Thus, the predictions made from the theoretical considerations related to the ground-state geometry of 24MBTO and the experimental findings from NMR measurements are in well agreement.

For understanding the ground-state CT complex formation mechanism and to show the donor and acceptor moiety effect on the spacer interaction, the bond length and bond angles are tabulated in Table 1. It is seen that the side-bond length of the spacer, C8−C11, is 1.332 Å compared to the standard value of

TABLE 1: Computed Values of Ground State Bond Lengths and Bond Angles of 24MBTO

	ground-state bond length (Å)	
	vacuum	ACN
C8−C11	1.332	1.332
C11−C12	1.458	1.458
	ground-state bond angle (degree)	
	vacuum	ACN
C9−C8−C11	121.2	121.2
C8−C11−C12	131.7	131.7
C11−C12−C17	117.9	117.9
C11−C12−C13	124.6	124.6
S7−C8−C11	128.4	128.4

TABLE 2: Ground State Dipole Moment of 24MBTO in Vacuum and ACN Medium

ground-state dipole moment (Debye)	
vacuum	ACN
4.1427	5.2832

1.34 Å and for C11−C12, it is 1.458 Å compared to the standard value of C−C single bond of 1.54 Å.

The bond length of the bichromophore is slightly less than the standard value for C8−C11 and highly decreased in case of C11−C12. This is the effect of torsional vibration of the different bonds and also electronic charge localization.

All are the predicted features of the through-bond coupling. Contraction of bonds signifies the donor and acceptor are not in ionic conditions. The coupling produces the delocalized orbitals; because of the mixing of the different symmetric and antisymmetric orbitals, the bond has a decrease in bond length. It is seen that the bond length and bond angles of the spacer part are not changing appreciably for a vacuum and in an ACN environment. This signifies that the atomic charges are redistributed to compensate the changes in bond lengths and bond angles.

(b) Dipole Moment. Asymmetric molecules generally have a dipole moment in the ground electronic state. Dipole moments for 24MBTO are calculated from the stable geometry for the ground state both in a vacuum and ACN solution by using the TD-DFT calculation. The values of dipole moments of 24MBTO in the vacuum are 4.1 and 5.3 D in ACN medium (Table 2). The increase of dipole moment signifies that significant CT between the donor (A) and the acceptor (T) parts of the molecule occurs, resulting in formation of loose-structured charge-separated species in highly polar ACN environment.

(c) Total Atomic Charge. From the optimized geometry of the molecule 24MBTO by the TD-DFT method, the total atomic charge distributions are computed and presented in Table 3. The spacer part comprises a double bond between C8−C11 and a single bond between C11−C12. From Table 3 it is observed that in C8 the charge is shifted from −0.331032 to −0.334693 and for C11 it is shifted from 0.037452 to 0.036217 and for C12 it is shifted from −0.091260 to −0.099374 for change in the environment from vacuum to ACN due to ground-state interatomic CT. In the case of C12, the magnitude of the charge shift is prominent, which is in accordance to the experimental observation of formation of the ground-state intramolecular CT absorption band in the polar ACN medium.

(d) Electronic Spectrum. From the computation (Table 4a) it is assigned that the HOMO is localized at molecular orbital no. 70 and LUMO is localized at molecular orbital no. 71. The first transition arise at 406 nm in a vacuum and at 411 nm in ACN environment by the two transitions from molecular orbital no.

TABLE 3: Total Atomic Charge Calculations of 24MBTO

atom no.	atom type	ground-state gas	ground-state ACN
1	C	−0.104971	−0.110727
2	C	−0.060863	−0.065940
3	C	−0.093766	−0.098737
4	C	−0.190253	−0.196788
5	C	−0.089742	−0.086604
6	C	0.013045	0.001557
7	S	0.247841	0.247089
8	C	−0.331032	−0.334693
9	C	0.290547	0.290071
10	O	−0.317121	−0.349135
11	C	0.037452	0.036217
12	C	−0.091260	−0.099374
13	C	−0.041066	−0.053175
14	C	−0.140048	−0.142573
15	C	0.194482	0.194025
16	C	−0.084527	−0.094427
17	C	−0.051191	−0.059275
18	O	−0.360895	−0.367013
19	C	−0.124241	−0.132941
20	H	0.101713	0.116842
21	H	0.102816	0.120836
22	H	0.094531	0.112299
23	H	0.103121	0.101794
24	H	0.121295	0.118725
25	H	0.103833	0.110699
26	H	0.102831	0.125784
27	H	0.106007	0.115396
28	H	0.095329	0.107925
29	H	0.115594	0.125686
30	H	0.115609	0.125587
31	H	0.134933	0.140872

69 → 71 and 70 → 71 or HOMO-1 to LUMO and HOMO−LUMO with oscillator strength 0.0286 and 0.0294, respectively, in a vacuum and in an ACN environment. The results are somehow in correlation with the experimentally observed ones.

The next transition arises at 373 nm in a vacuum and 361 nm in ACN by 68 → 71 molecular orbital transition with a very negligible oscillator strength.

The next transition arises at 339 nm in a vacuum and at 348 nm in an ACN environment by the two transitions from molecular orbital no. 69 → 71 and 70 → 71 with oscillator strength 0.0393 and 0.0394, respectively, in a vacuum and in ACN environment. The results are in good agreement with the experimentally observed transition of 345 nm.

The next prominent transition arises at 271 nm in a vacuum by the three transitions from molecular orbital no. 66 → 71, 67 → 71, and 70 → 72 with oscillator strength 0.0340 and in ACN environment by the two transitions from molecular orbital no. 66 → 71 and 70 → 72 with oscillator strength 0.0365. The peak is very prominent in the theoretically observed molecular spectra.

The other prominent transition arises at 259 nm in a vacuum by the four transitions from molecular orbital no. 66 → 71, 67 → 71, 70 → 73, and 70 → 74 with oscillator strength 0.0202 and 256 nm in ACN environment by the five transitions from molecular orbital no. 65 → 71, 67 → 71, 67 → 72, 70 → 73, and 70 → 74 with oscillator strength 0.0236. The results are in good agreement with the experimentally observed transition of 256 nm.

3.2. Measurement of Steady-State Fluorescence Emission Spectra. On direct excitation of the CT absorption band ($\lambda_{ex} \approx$ 438 nm) of 24MBTO in ACN, an overlapping of the two fluorescence emission spectra, one peaking at 500 nm and another one at around 600 nm, was found (Figure 4). These observations demonstrate that the two emissions may possibly be due to the formations of two different types of isomers:

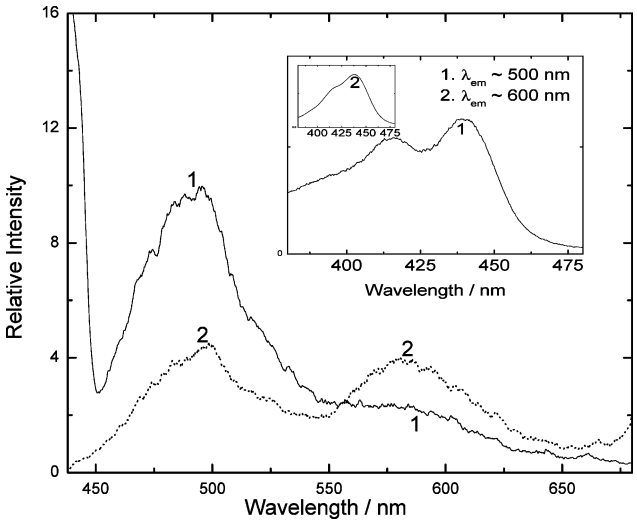

Figure 4. Steady-state fluorescence emission spectra of 24MBTO in ACN at the ambient temperature when the excitation wavelengths used in (1) 438 nm and (2) 345 nm. (Inset) Steady-state fluorescence excitation spectra of the two fluorescence emission bands, produced by exciting with 438 nm, at 500 and 600 nm.

Z-type and E-type resulted from CT reactions. Although ground-state NMR study indicates that in the ground state, mainly the Z-isomer exists, upon excitation of the Z-form by UV light, it appears that some Z-forming species may be transformed into the E-isomeric form. The augmentation of the longer wavelength emission band at 600 nm is observed at the expense of 500-nm emission due to the change of the location of excitation from the lower-energy region (∼438 nm) of stable Z-isomeric species to higher one (∼345 nm) of the absorption band of 24MBTO. This observation demonstrates that the longer wavelength CT emission band resided at 600-nm region should not be due to Z-isomers but is mostly due to another isomeric form, E-types.

There is a possibility that in the ground state these species being conformationally unstable relative to the Z-isomer absorb at the higher-energy region. Thus, the experimental findings reveal that in the lowest excited-singlet state, E-isomeric species becomes more stable (emits at the longer wavelength side) than the other Z-isomeric species, unlike the situation in the ground state where the latter isomers appear to possess a more-stable configuration.

Thus, from the above observations it appears that the present thioaurone may behave as a photoswitchable system because, due to excitation in the region of 410−450 nm, where only Z-isomeric species largely predominates, the 600-nm emission band, presumably due to E-isomeric species, also develops along with the 500-nm fluorescence band of the Z-isomer. Moreover, the fluorescence excitation spectra of the two fluorescence bands at 500 and 600 nm were measured and reproduced in the insets of the Figure 4. The observed similar excitation spectra, which correspond well to the UV−vis spectra of CT absorption band resided within the 400−460-nm region, demonstrate that both the emitting species have the one ground-state precursor (z-isomer). Under photoirradiation or photoexcitation, some ground-state Z-forms convert into excited-state E-isomeric species.

However, the geometry and vertical transition calculations were also carried out for E-isomer to find out its vertical excitation using the calculated heat of formation and entropy term as was done (discussed above) in the case of the other isomer, Z. The values are shown in Table 4b. From the table, it is apparent that in ACN environment, only Z-isomers prevail in the 410-nm band region of the absorption spectra, whereas

TABLE 4[a]

(a) Theoretical and experimental data for 24MBTO in a vacuum and ACN solvent

vacuum				ACN			
excitation	C.I expansion coefficient	wavelength (nm)	*f*	excitation	C.I expansion coefficient	wavelength (nm)	*f*
69 → 71	0.19190	405.82	0.0286	69 → 71	0.20786	410.78	0.0294
70 → 71	0.57382			70 → 71	0.56656	(438)[b]	
68 → 71	0.66781	373.41	0.0000	68 → 71	0.67031	361.33	0.0000
69 → 71	0.62564	338.73	0.0393	69 → 71	0.61927	347.64	0.0394
70 → 71	−0.16725			70 → 71	−0.18473	(345)[b]	
66 → 71	0.55664	286.33	0.0046	67 → 71	0.63838	292.16	0.0029
67 → 71	−0.10116			70 → 72	−0.12734		
70 → 72	−0.28456			70 → 73	0.17192		
70 → 73	0.27281			70 → 74	−0.14545		
67 → 71	0.45713	278.02	0.0050	66 → 71	0.54869	278.82	0.0019
69 → 72	−0.13737			67 → 71	−0.11519		
70 → 72	−0.40205			69 → 72	−0.13467		
70 → 74	0.19493			70 → 72	−0.26567		
				70 → 74	0.12541		
66 → 71	0.26026	270.55	0.0340	66 → 71	0.29431	270.65	0.0365
67 → 71	0.39859			70 → 72	0.57338		
70 → 72	0.42513						
69 → 75	0.15006	260.36	0.0001	69 → 75	0.16803	257.97	0.0000
70 → 75	0.66715			70 → 75	0.66347		
66 → 71	0.27200	259.11	0.0202	65 → 71	0.11913	256.60	0.0236
67 → 71	−0.11241			67 → 71	−0.19594	(256.00)[b]	
70 → 73	−0.54376			67 → 72	−0.11410		
70 → 74	0.18852			70 → 73	0.48069		
				70 → 74	−0.36433		
65 → 71	0.14845	255.90	0.0002	65 → 71	0.40438	255.45	0.0015
69 → 72	0.12027			70 → 73	0.24407		
70 → 73	0.19803			70 → 74	0.44828		
70 → 74	0.58986						
65 → 71	0.62781	249.13	0.0096	65 → 71	0.48837	252.09	0.0057
70 → 74	−0.11123			69 → 72	−0.14908		
				70 → 73	−0.30634		
				70 → 74	−0.26245		

(b) Comparison of the theoretical data between Z- and E-isomers both in gas phase and ACN environment

vacuum/gas phase (Z-isomer)			ACN environment (Z-isomer)			ACN environment (E-isomer)		
excitation	wavelength (nm)	oscillator strength	excitation	wavelength (nm)	oscillator strength	excitation	wavelength (nm)	oscillator strength
69 → 71	405.82	0.0286	69 → 71	410.78	0.0294	69 → 71		
70 → 71			70 → 71	(438)[b]		70 → 71		
68 → 71	373.41	0.0000	68 → 71	361.33	0.0000	67 → 71	396.93	0.0013
						68 → 71		
						69 → 71		
69 → 71	338.73	0.0393	69 → 71	347.64	0.0394	67 → 71	353.84	0.0335
70 → 71			70 → 71	(345)[b]		68 → 71		
						69 → 71		
						70 → 71		
66 → 71	286.33	0.0046	67 → 71	292.16	0.0029	67 → 71	307.15	0.0007
67 → 71			70 → 72			68 → 71		
70 → 72			70 → 73			70 → 73		
70 → 73			70 → 74					
67 → 71	278.02	0.0050	66 → 71	278.82	0.0019	66 → 71	286.67	0.0016
69 → 72			67 → 71			69 → 72		
70 → 72			69 → 72			70 → 72		
70 → 74			70 → 72			70 → 74		
			70 → 74					

[a] "*f*" denotes oscillator strength. [b] Experimental values in ACN medium.

nearly equal contributions of Z- and E-isomers (similar *f*-values) were observed in the 347-nm region of the absorption band. This is actually what we observed experimentally. As is apparent from Figure 4, the augmentation of the fluorescence band at 600 nm, which is responsible for the E-isomeric species, occurs due to a change of excitation from the 438- to 345-nm position. It is to be mentioned here that excitation using 438-nm wavelength (Figure 4), which situates in the region of the Z-isomer, leads to formations of both the emission bands at 500 and 600 nm, of which the latter one is due to formation of E-isomeric species by photoswitchable effect. The larger emission intensity at 500 nm indicates that even after photoexcitation to the lowest excited singlet state, a significant fraction of the Z-form still remains.

In case of Z-isomer, the sum of electronic and thermal enthalpies is −1165.508292 Hartree per particle and entropy is

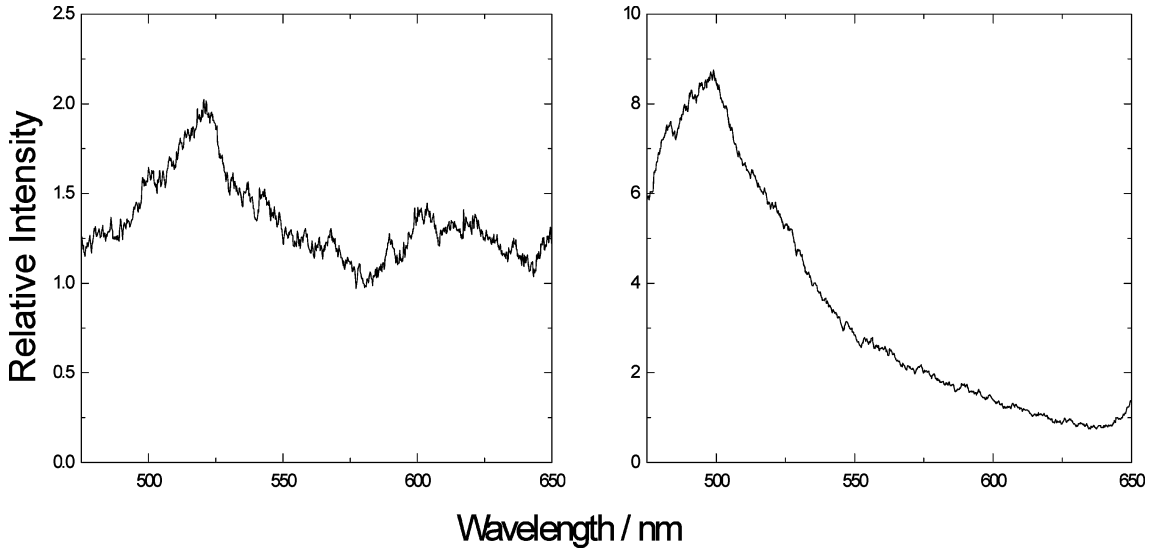

Figure 5. Steady-state fluorescence emission spectra of 24MBTO in aqueous medium without βCD (left) and with a large concentration ($\sim 10^{-2}$ mol dm^{-3}) of βCD (right).

117.686 cal/mol. Kelvin. Whereas, for E-isomer the sum of electronic and thermal enthalpies is −1165.500240 hartree per particle and entropy is 124.773 cal/mol K. Thus, from the calculations of heat of formation and entropy term, the ground-state equilibrium constant between Z- and E-isomers is computed to be 143.6. Therefore, it is assigned that the percentage of Z-isomer is 99.31% in the ground state. Thus, the theoretical predictions correlate well with the experimental findings from NMR as well as steady-state spectroscopic studies that Z-isomers predominate in the ground state.

Further Investigations on the Excited Isomeric Species Using βCD Microenvironment. In aqueous medium, 24MBTO exhibits similar overlapping of the two emission bands residing nearly at the same energy regions, as was observed in ACN environment. The shorter wavelength emission that appears to be due to the Z-isomeric species was found to be enhanced with increasing concentrations of βCD (Figure 5). From the figure it is apparent that at a large concentration ($\sim 10^{-2}$ mol dm^{-3}) of βCD, the 600-nm band completely disappears and only the 500-nm fluorescence emission exists. This shows that, due to encapsulation of the bichromophore within βCD, the formation of inclusion complex of Z-form with βCD is largely facilitated. This experimental observation demonstrates that the geometrical constraints imposed by the nonpolar cavity of βCD on the photogenerated species (both Z- and E- forms) facilitate the survival of the Z-form only. As from the theoretical predictions, it appears that the structure of the Z-isomeric species is more-or-less elongated (not folded type, Figure 1b); thus, this species could easily be incorporated within the βCD cavity. Though the exact molecular structure of the E-isomeric form is not very clear from the present stage of investigation, it could be conjectured that E-form may possess relatively folded type geometry and, thus, becomes unable to form any inclusion complex with βCD. Thus, for the formation of inclusion complex, E-isomeric species should be converted into the more elongated Z-form.

3.3. Temperature Effect on the Stability of Two Isomers. With a gradual increase of temperature from 305 to 342 K, the fluorescence intensity of 24MBTO in ACN at the lower wavelength region (corresponding to Z-isomer) decreases, whereas marginal change in intensity was found in the fluorescence band system residing in the domain of higher wavelengths (region of E-isomer) (Figure 6). This is in accord to our expectation, as the E -isomer is energetically more stable in the excited state, whereas in the ground state, the stability of Z-form is much higher.

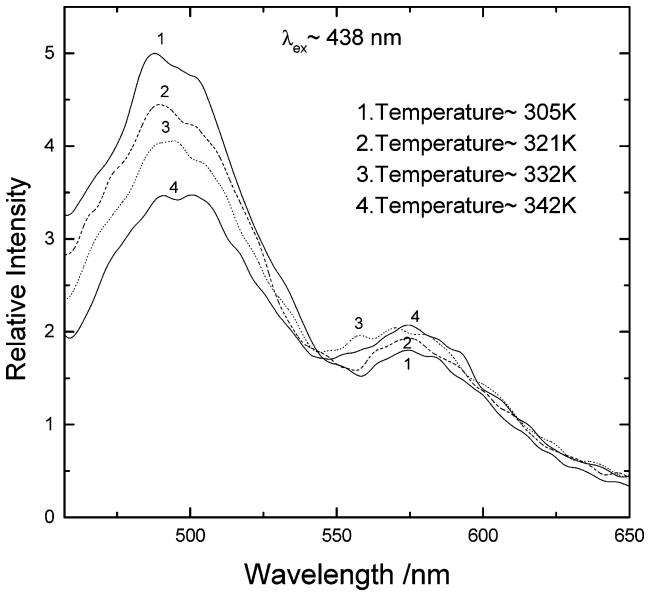

Figure 6. Steady-state fluorescence emission spectra of 24MBTO in ACN ($\lambda_{ex} \approx 438$ nm) at the different temperatures.

3.4. Effect of pH on the Isomers. The investigations on the effect of pH on the CT emission of 24MBTO yield very interesting results. Upon gradually increasing or decreasing the pH of the environment, only one isomer, which emits in the shorter wavelength region ($\sim$500 nm, Z-isomer), dominates. A plausible interpretation is that with gradual addition of acid, the carbonyl group in the thioindoxyl part of 24MBTO is protonated. As a result, the double bond linker existing between A and T reduces to a more flexible single bond, causing free rotation of the donor and acceptor moieties. As a result, various conformations might result. Nevertheless, from the experimental findings, it appears that there is a preponderance of the Z-form (Figure 7a); with a gradual decrease of pH, the 500-nm band becomes more and more prominent relative to the 600-nm emission band, which has been assigned due to the formation of E-isomeric species.

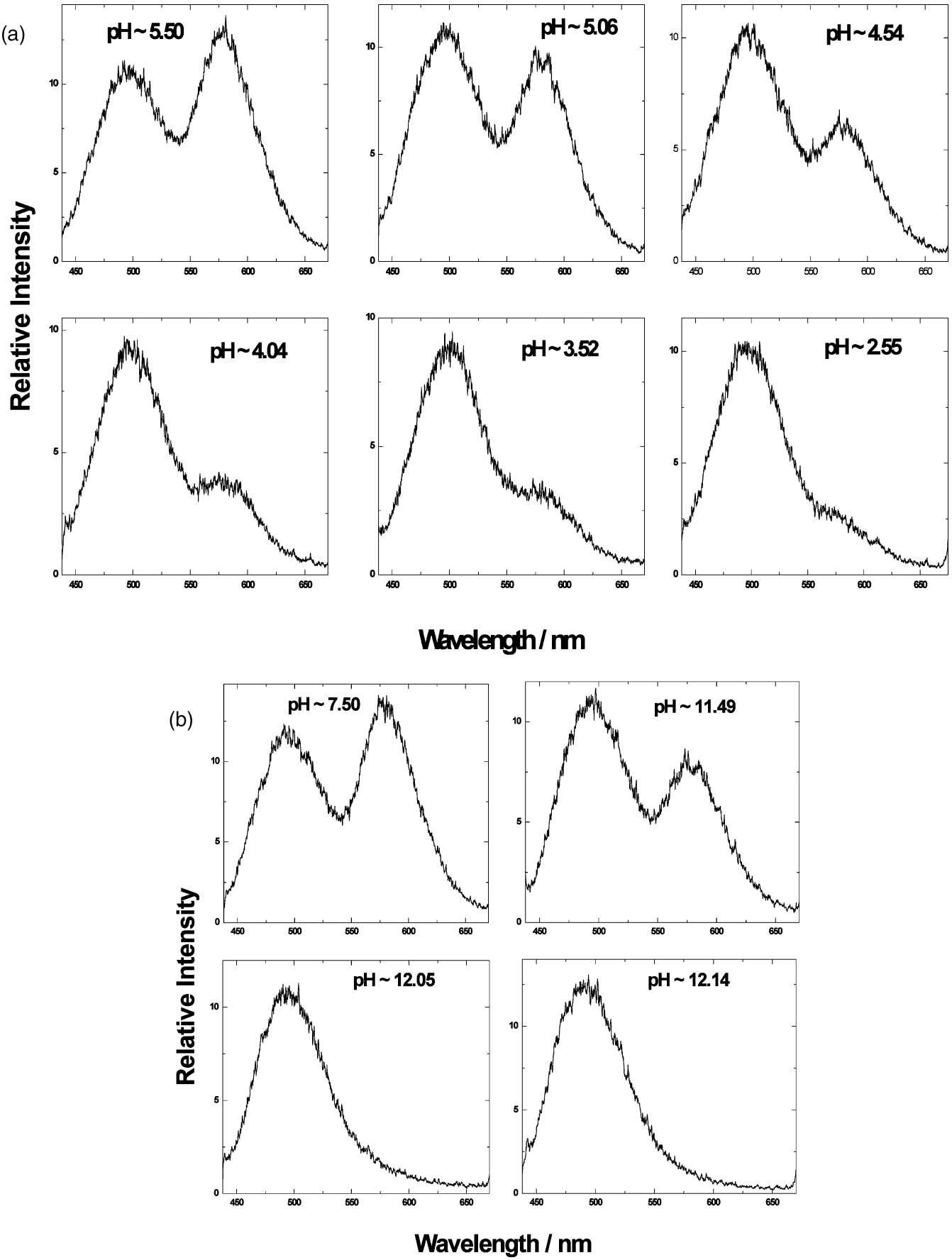

Figure 7. (a) Changes observed in the steady-state fluorescence emission spectra of the two isomeric species of 24MBTO (Z- and E-) in ACN due to a lowering of the pH of the environment (acidic region). (b) Changes observed in the steady-state fluorescence emission spectra of the two isomeric species (Z- and E-) of 24MBTO in ACN due to an increase in the pH of the environment (alkaline region).

TABLE 5: Fluorescence Lifetime Values of 24MBTO along with the Fractional Contributions (f_i)[a] in Different Media at the Ambient Temperature

medium	λ_{em}/nm[b]	τ_1/ns	τ_2/ns	f_1	f_2
ACN	500	1.4			
	550	1.6			
	600	1.1	6.0	0.06	0.94
aqueous	550	0.4	4.0	0.52	0.48
aqueous + βCD[c]	550	0.5			

[a] $f_i = a_i\tau_i/\Sigma a_j\tau_j$ ($a \approx$ normalized preexponential factor, see text). [b] Excitation wavelength: 405 nm ($\lambda_{em} \approx$ monitoring wavelengths). [c] Decay becomes single exponential and analysis yields only the lower component (~0.5 ns) of the two lifetimes observed in aqueous medium without βCD.

The similar observations of survival of Z-form only were made in alkaline medium also (Figure 7b). As it was proposed in the case of acidic medium, the transformation of the double bond linker existing within 24MBTO between T and A moieties to a more flexible single one facilitates with an increase of alkalinity of the surrounding medium, and the relatively free rotations of the donor and acceptor moieties produce larger amount of Z-isomers, relative to the other isomeric species E, in the excited singlet S1.

3.5. Fluorescence Lifetime Measurements In ACN Medium. The fluorescence lifetime measurements of 24MBTO were made by exciting at $\lambda_{ex} \approx 405$ nm (corresponding to the CT band), and fluorescence decays were measured by monitoring at $\lambda_{em} \approx 500$, 550, and 600 nm. From the lifetime measurements (values are shown in Table 5), the single fluorescence decay of 24MBTO was observed when monitored at $\lambda_{em} \approx 500$ (the region of Z-isomers) and 550 nm. In both cases, the values of the lifetimes are close enough (~1.5 ns), so it should correspond to one isomer (the Z-form). But when the fluorescence decay was monitored at $\lambda_{em} \approx 600$ nm (the region of mostly E-isomeric species), the decay becomes biexponential, the analysis of which yields the two lifetime components, 1.1 ns (τ_1) and 6 ns (τ_2), among which the longer component has the major contribution ($f_2 \approx 0.94$, Table 5). As this lifetime (τ_2), appears to be present only in the emission band of the longer wavelength region; this should logically be due to the E- isomer, which was found to be more stable in the excited state relative to the Z-isomer from steady-state measurements. Another lifetime τ_1 (~1.1 ns) is very similar to the lifetime observed when monitoring in the domain of Z-isomer (around 500-nm region) only. As expected, at the 600-nm region, the fractional contribution[33−35] of this Z-species becomes very small ($f_1 \approx 0.06$) and the dominant contribution ($f_2 \approx 0.94$, Table 5) of the other isomeric species (E-form, ~6 ns) is apparent from lifetime measurements.

Further Investigations on Fluorescence Lifetimes Using βCD Microenvironment. It was discussed in Section 3.2 that steady-state fluorescence measurements demonstrate that in aqueous medium, 24MBTO exhibits similar overlapping of the two emission bands residing nearly at the same energy regions as was observed in ACN environment. The fluorescence emission band resided at the shorter wavelength region (~500 nm), which appears to be due to the Z-isomeric species that was found to be enhanced in the presence of βCD (Figure 5). Time-resolved spectroscopic investigations made in aqueous medium, both in the absence and presence of βCD, yield similar results.

In aqueous medium, at the 550-nm region, 24MBTO exhibits two fluorescence lifetimes. Both the shorter and longer components were found to be relatively lower in magnitudes (~0.4 and 4 ns, respectively, Table 5) than the corresponding values observed in ACN. As is apparent from the steady-state spectra (Figure 5), at the 550-nm region, nearly equal fractional contributions (~0.5, Table 5) of the two species were found from lifetime measurements. The situation drastically changes in the presence of βCD, where the decay at 550 nm exhibits clearly single exponential and the analysis of which yields 0.5 ns, which corresponds to the lower component observed in aqueous medium, and the longer one completely disappears. The time-resolved measurements reveal that in the presence of βCD, the Z-isomeric species prevails. Thus, time-resolved spectroscopic results corroborate significantly with the views made from the steady-state measurements.

Thus, the present steady-state and time-resolved spectroscopic measurements demonstrate that under photoirradiation, reversible E/Z isomerization occurs. The similar situation was observed in cases of a chiral polyamidoamine side chain dendritic polyester.[36] The present observations indicate that 24MBTO bichromophoric system may behave as a versatile photoswitchable system.[37] Moreover, the relative yields of the two photoproducts (Z and E isomers), resulting from charge-separation reactions, could be controlled by changing the temperature, pH, and nature of the surrounding medium.

Although in the excited singlet state E-isomeric form is found to be relatively more stable than the Z-isomer, by using a βCD microenvironment, most of the E-isomeric species have been converted into its Z-form through formation of inclusion complexes, as the latter species is structurally elongated in nature. Such elongation will keep the donor and acceptor parts at a far-apart position and refrain them from overlapping with each other. This will minimize the energy wasting process charge recombination occuring within this encapsulated product.

Concluding Remarks

Both steady-state and time-resolved measurements on the novel synthesized 24MBTO demonstrate that both in the ground and excited electronic states, two types of isomer, E- and Z-forms, are formed as a result of the charge separation reactions. Though in the ground-state Z-form is found to be more stable from energetic consideration, interestingly, the excited-state measurements reveal the formations of more stable E-isomeric species along with Z-isomers in the electronic excited state. Thus, under photoirradiation, reversible Z/E isomerization occurs, as was observed in cases of a chiral polyamidoamine side chain dendritic polyester. These observations demonstrate that the present thioaurone system may behave as a versatile photoswitchable system. The relative yields of the two photoproducts (Z- and E-isomers) could be controlled by changing the temperature, pH, and the nature of the surrounding medium. In βCD microenvironment, most of the E-isomeric species have been converted into its Z-form through formation of inclusion complexes, as the latter species is structurally elongated in nature. Such elongation will keep the two redox centers, donor and acceptor parts, at a far-apart position. The geometrical constraints imposed by the cavity refrain the two redox parts from overlapping with each other. This will minimize the energy wasting or loss process charge recombination to occur within this encapsulated product.

Acknowledgment. We thankfully acknowledge the cooperation of Professor Kankan Bhattacharyya for allowing us to use the Pico/Femtosecond laser facility, sponsored by the Department of Science and Technology (DST) (Project No. IR/I-1/CF-01/2002), Govt. of India, for recording the fluorescence decays. S.R.C. thanks the University Grants Commission

(UGC), New Delhi, and T.G. acknowledges the financial support provided by the Department of Science and Technology (DST) (Project No. SR/S1/PC-17/2003), New Delhi in the form of grants and fellowships.

References and Notes

(1) (a) Paddon-Row, M. N. In *Electron-Transfer in Chemistry*; Balzani, V., Ed.; Wiley-VCH: Weinheim, Germany **2001**; Vol. 3, Part 2, Chapter 1, p 179. (b) Seischal, M.; Lodenkemper, T.; Stockman, A.; Schmeider, S.; Koeberg, M.; Roest, M. R.; Verhoeven, J. W.; Lawson, J. M.; Paddon-Row, M. N. *Phys. Chem. Chem Phys.* **2000**, *2*, 1889 (c) Pal, S. K.; Bhattacharya, T.; Misra, T.; Saini, R. D.; Ganguly, T. *J. Phys. Chem. A* **2003**, *107*, 10243: (d) Pal, S. K.; Sahu, T.; Misra, T.; Mallick, P. K.; Paddon-Row, M. N.; Ganguly, T. *J. Phys. Chem. A* **2004**, *108*, 10395.

(2) Pal, S. K.; Sahu, T.; Misra, T.; Ganguly, T.; Pradhan, T. K.; De, A. *J. Photochem. Photobiol. A: Chem.* **2005**, *174*, 138.

(3) Imahori, H.; El-Khouly, M. E.; Fijitsuka, M.; Ito, O.; Sakata, Y.; Fukuzumi, S. *J. Phys. Chem. A* **2001**, *105*, 325.

(4) Imahori, H.; Norieda, H.; Yamada, H.; Nishimura, Y.; Yamazaki, I.; Sakata, Y.; Fukuzumi, S. *J. Am. Chem. Soc.* **2001**, *123*, 100.

(5) Paddon-Row, M. N. *Adv. Phys. Org. Chem.* **2003**, *38*, 1.

(6) van der Boom, T.; Hayes, R. T.; Zhao, Y.; Bushard, P. J.; Weiss, E. A.; Wasielewski, M. R. *J. Am. Chem. Soc.* **2002**, *124*, 9582.

(7) Davis, W. B.; Ratner, M. A.; Wasielewski, M. R. *Chem. Phys.* **2002**, *281*, 333.

(8) Shaakov, S.; Galini, T.; Stavitski, E.; Levanon, H.; Lukas, A.; Wasielewski, M. R. *J. Phys. Chem. A* **2003**, *125*, 6363.

(9) Heinen, U.; Berthold, T.; Kothe, G.; Stavitski, E.; Galini, T.; Levanon, H.; Wiederrecht, G.; Wasielewski, M. R. *J. Phys. Chem. A* **2002**, *106*, 1933.

(10) Blank, A.; Galini, T.; Levanon, H. *J. Porphyrins Phthalocyanines* **2001**, *5*, 58.

(11) Berg, A.; Shuali, Z.; Asano-Someda, M.; Levanon, H.; Fuhs, M.; Möbius, K. *J. Am. Chem. Soc.* **1999**, *121*, 7433.

(12) Wasielewski, M. R.; Niemczyk, M. P.; Svec, W. A.; Pewitt, E. B. *J. Am. Chem. Soc.* **1985**, *107*, 1080.

(13) Wasielewski, M. R.; Niemczyk, M. P.; Svec, W. A.; Pewitt, E. B. *J. Am. Chem. Soc.* **1985**, *107*, 5562.

(14) Levanon, H. *RiKEN Rev.* **1999**, *24*, 38.

(15) Asano-Someda, M.; Levanon, H.; Sessler, J. L.; Wang, R. *Mol. Phys.* **1998**, *95*, 935.

(16) Loken, N.; Paddon-Row, M. N.; Smith, T. A.; La Rosa, M.; Ghiggino, K. P. *J. Am. Chem. Soc.* **1999**, *121*, 2917.

(17) Paddon-Row, M. N. *Aust. J. Chem.* **2003**, *56*, 729.

(18) Ghiggino, K. P.; Clayton, A. H. A.; Lawson, J. M.; Paddon-Row, M. N. *New. J. Chem.* **1996**, *20*, 853.

(19) Bell, T. D. M.; Jolliffe, K. A.; Ghiggino, K. P.; Oliver, A. M.; Shephard, M. J.; Langford, S. J.; Paddon-Row, M. N. *J. Am. Chem. Soc.* **2002**, *106*, 10079.

(20) Bell, T. D. M.; Ghiggino, K. P.; Jolliffe, K. A.; Ranasighe, M. G.; Langford, S. J.; Shephard, M. J.; Paddon-Row, M. N. *J. Phys. Chem. A* **2002**, *106*, 1933.

(21) Bell, T. D. M.; Smith, T. A.; Ghiggino, K. P.; Ranasighe, M. G.; Shephard, M. J.; Paddon-Row, M. N. *Chem. Phys. Lett.* **1997**, *268*, 233.

(22) De Schryver, F. C.; Declereq, D.; Depaemelaere, S.; Hermans, E.; Onkelinx, A.; Verhoeven, J. W. *J. Photochem. Photobiol. A: Chem.* **1994**, *82*, 171.

(23) Ganguly, T.; Sharma, D. K.; Gauthier, S.; Gravel, D.; Durocher, G. *J. Phys. Chem.* **1992**, *96*, 3757.

(24) Staab, H. A.; Weiser, J.; Baumann, E. *Chem. Ber.* **1992**, *125*, 2275.

(25) Gust, D.; Moore, T. A. In *Advances in Photochemistry*; Volman, D. H., Hammond, G. S., Neckers, D. C., Eds.; Wiley: New York, 1991; p 1.

(26) Maiti, M.; Misra, T.; Bhattacharya, T.; Basu, C.; De, A.; Sarkar, S.K.; Ganguly, T. *J. Photochem. Photobiol. A: Chem.* **2002**, *152*, 41

(27) Misra, T.; Bhattacharya, T.; Pal, S. K.; De, A.; Saini, R. D.; Ganguly, T. *Chem. Phys. Lett.* **2003**, 382, 167

(28) Morzek, J.; Guzow, K.; Szabelski, M.; Karolczak, J.; Wiczk, W. *J. Photochem. Photobiol. A: Chem.* **2002**, *153*, 121

(29) Becke, A. D. *J. Chem. Phys.* **1993**, *98*, 5648.

(30) Cox, A. P.; Riveros, J. M. *J. Chem. Phys.* **1965**, *42*, 3106.

(31) Peterson, G. A.; Al-Laham, M. A. *J. Chem. Phys.* **1991**, *94*, 6081.

(32) Frisch, M. J.; Trucks, G. W.; Schlegel, H. B.; Scuseria, G. E.; Robb, M. A.; Cheeseman, J. R.; Zakrzewski, V. G.; Montgomery, J. A., Jr.; Stratmann, R. E.; Burant, J. C.; Dapprich, S.; Millam, J. M.; Daniels, A. D.; Kudin, K. N.; Strain, M. C.; Farkas, O.; Tomasi, J.; Barone, V.; Cossi, M.; Cammi, R.; Mennucci, B.; Pomelli, C.; Adamo, C.; Clifford, S.; Ochterski, J.; Petersson, G. A.; Ayala, P. Y.; Cui, Q.; Morokuma, K.; Malick, D. K.; Rabuck, A. D.; Raghavachari, K.; Foresman, J. B.; Cioslowski, J.; Ortiz, J. V.; Stefanov, B. B.; Liu, G.; Liashenko, A.; Piskorz, P.; Komaromi, I.; Gomperts, R.; Martin, R. L.; Fox, D. J.; Keith, T.; Al-Laham, M. A.; Peng, C. Y.; Nanayakkara, A.; Gonzalez, C.; Challacombe, M.; Gill, P. M. W.; Johnson, B. G.; Chen, W.; Wong, M. W.; Andres, J. L.; Head-Gordon, M.; Replogle, E. S.; Pople, J. A. *Gaussian 98*, revision A.7; Gaussian, Inc.: Pittsburgh, PA, 1998**.**

(33) Steinle, W.; Ruck-Braun, K. *Org. Lett.* **2003**, 141.

(34) Ganguly, T.; Farmer, L.; Gravel, D.; Durocher, G. *J. Photochem. Photobiol. A: Chem.* **1991**, *60*, 63.

(35) Sahu, T.; Pal, S. K.; Misra, T.; Ganguly, T. *J. Photochem. Photobiol. A: Chem.* **2005**, *171*, 39

(36) Villavicencio, O. F.; McGrath, D. V. In *Advances in Dendritic Macromolecules*; Newkome, G. R., Ed.; JAI Press: Greenwich, CT, 2002, Vol. 5, pp 1−44.

(37) Junge, D. M.; Mcgrath, D. V. *J. Am. Chem. Soc.* **1999**, *121*, 4912.